JGR Atmospheres

RESEARCH ARTICLE
10.1029/2023JD039159

Highly Hygroscopic Aerosols Facilitate Summer and Early-Autumn Cloud Formation at Extremely Low Concentrations Over the Central Arctic Ocean

P. Duplessis[1], L. Karlsson[2,3], A. Baccarini[4,5], M. Wheeler[6], W. R. Leaitch[7], B. Svenningsson[8], C. Leck[3,9], J. Schmale[4], P. Zieger[2,3], and R. Y.-W. Chang[1]

[1]Department of Physics and Atmospheric Science, Dalhousie University, Halifax, NS, Canada, [2]Department of Environmental Science, Stockholm University, Stockholm, Sweden, [3]Bolin Centre for Climate Research, Stockholm University, Stockholm, Sweden, [4]Extreme Environments Research Laboratory, École Polytechnique fédérale de Lausanne, Sion, Switzerland, [5]Now at Laboratory for Atmospheric Processes and their Impact, École Polytechnique fédérale de Lausanne, Lausanne, Switzerland, [6]Air Quality Division, Environment and Climate Change Canada, Toronto, ON, Canada, [7]Climate Research Division, Environment and Climate Change Canada, Toronto, ON, Canada, [8]Department of Physics, Lund University, Lund, Sweden, [9]Department of Meteorology, Stockholm University, Stockholm, Sweden

Key Points:

- Aerosol hygroscopicity was greater after surface water freeze-up than before
- Hygroscopicity of Aitken mode particles was generally greater than accumulation mode particles
- Cloud droplet effective radii during aerosol-limited periods were larger generally than periods with higher aerosol concentrations

Supporting Information:

Supporting Information may be found in the online version of this article.

Correspondence to:

R. Y.-W. Chang and P. Zieger,
rachel.chang@dal.ca;
Paul.Zieger@aces.su.se

Citation:

Duplessis, P., Karlsson, L., Baccarini, A., Wheeler, M., Leaitch, W. R., Svenningsson, B., et al. (2024). Highly hygroscopic aerosols facilitate summer and early-autumn cloud formation at extremely low concentrations over the central Arctic Ocean. *Journal of Geophysical Research: Atmospheres*, *129*, e2023JD039159. https://doi.org/10.1029/2023JD039159

Received 26 APR 2023
Accepted 22 DEC 2023

Author Contributions:

Conceptualization: P. Duplessis, L. Karlsson, M. Wheeler, W. R. Leaitch, C. Leck, J. Schmale, P. Zieger, R. Y.-W. Chang
Data curation: P. Duplessis, L. Karlsson, A. Baccarini
Formal analysis: P. Duplessis, L. Karlsson, A. Baccarini
Funding acquisition: P. Duplessis, M. Wheeler, W. R. Leaitch, C. Leck, J. Schmale, P. Zieger, R. Y.-W. Chang

Abstract Arctic clouds are sensitive to atmospheric particles since these are sometimes in such low concentrations that clouds cannot always form under supersaturated water vapor conditions. This is especially true in the late summer, when aerosol concentrations are generally very low in the high Arctic. The environment changes rapidly around freeze-up as the open waters close and snow starts accumulating on ice. We investigated droplet formation during eight significant fog events in the central Arctic Ocean, north of 80°, from August 12 to 19 September 2018 during the Arctic Ocean 2018 expedition onboard the icebreaker *Oden*. Calculated hygroscopicity parameters (κ) for the entire study were very high (up to $\kappa = 0.85 \pm 0.13$), notably after freeze-up, suggesting that atmospheric particles were very cloud condensation nuclei (CCN)-active. At least one of the events showed that surface clouds were able to form and persist for at least a couple hours at aerosol concentrations less than 10 cm^{-3}, which was previously suggested to be the minimum for cloud formation. Among these events that were considered limited in CCN, effective radii were generally larger than in the high CCN cases. In some of the fog events, droplet residuals particles did not reactivate under supersaturations up to 0.95%, suggesting either in-droplet reactions decreased hygroscopicity, or an ambient supersaturation above 1%. These results provide insight into droplet formation during the clean late-summer and fall of the high Arctic with limited influence from continental sources.

Plain Language Summary The Arctic atmosphere can be very clean in the summer, to the point that clouds cannot form because there are insufficient particles present for the water vapor to condense upon. This has important implications for the radiation budget, which is highly dependent on clouds. As part of the Arctic Ocean 2018 expedition in the central Arctic Ocean near the North Pole, we investigated the ability of particles to turn into droplets throughout the whole cruise (August 12 to 19 September 2018), and during eight significant fog events. Overall, we found that after the sea ice started to freeze, the particles were more capable of turning into cloud droplets. During one fog event, we observed fog droplets forming when the particle concentrations were lower than the limit that past studies had suggested that fog/cloud could be sustained. During several fog events, the dried fog droplets did not always re-form droplets when exposed to cloud-like conditions, which suggests that the original droplets must have formed under extreme conditions. Our results show that in the summer/fall in the high Arctic, liquid droplets sometimes form under unusual circumstances that are likely not always considered in models.

1. Introduction

Due to complex feedback mechanisms, aerosol-cloud interactions remain a large part of the uncertainties in future climate projections (IPCC, 2022). Clouds affect the global radiation budget and, in turn, modulate the faster warming of the Arctic, also known as Arctic amplification (Rantanen et al., 2022), which is closely tied to the sea-ice extent (Screen & Simmonds, 2010). Clouds are critical in modulating the radiative components of the surface energy budget, which is essential to the changing Arctic in all seasons, especially the melting and freezing of the perennial sea ice. In contrast to their mid-latitude and/or subtropical counterparts, known to cool

Investigation: P. Duplessis, L. Karlsson, A. Baccarini, M. Wheeler, J. Schmale, P. Zieger, R. Y.-W. Chang
Methodology: P. Duplessis, L. Karlsson, M. Wheeler, W. R. Leaitch, B. Svenningsson, C. Leck, J. Schmale, P. Zieger, R. Y.-W. Chang
Project Administration: P. Duplessis, C. Leck, J. Schmale, P. Zieger, R. Y.-W. Chang
Resources: P. Duplessis, M. Wheeler, W. R. Leaitch, B. Svenningsson, C. Leck, J. Schmale, P. Zieger, R. Y.-W. Chang
Software: P. Duplessis, L. Karlsson
Supervision: P. Duplessis, P. Zieger, R. Y.-W. Chang
Validation: P. Duplessis, L. Karlsson, A. Baccarini
Visualization: P. Duplessis, L. Karlsson
Writing – original draft: P. Duplessis, L. Karlsson, C. Leck, J. Schmale, R. Y.-W. Chang
Writing – review & editing: P. Duplessis, L. Karlsson, A. Baccarini, M. Wheeler, W. R. Leaitch, B. Svenningsson, C. Leck, J. Schmale, P. Zieger, R. Y.-W. Chang

the climate system, low-level clouds in the high Arctic mostly warm the surface, as the surface reflectivity is as high as, or higher than, the cloud albedo. However, in the most intense summer ice melt, the surface reflectivity can be reduced by the opening of leads and by the formation of melt ponds on the ice, and then low-level clouds may lead to surface cooling for a short period (Intrieri et al., 2002; Sedlar et al., 2011; Shupe & Intrieri, 2004).

The high Arctic region, here defined as north of 80°, also has a strong seasonal contrast throughout the year, not only because of the temperature and sea ice conditions but because of the perpetual sunlight in summer and the long polar night in winter (Schmale et al., 2021). These conditions introduce significantly different atmospheric transport dynamics and atmospheric chemical reactions, which impact cloud formation differently (Schmale et al., 2021; Stohl, 2006). As a result, the summer atmosphere over the central Arctic Ocean is separated mainly from air masses associated with strong sources of pollution. As such, the optical properties of the Arctic low-level clouds are often optically thin, with fewer but larger droplets compared to other regions (e.g., Tjernström et al., 2008).

Summertime cloud condensation nuclei (CCN) concentrations can be so low at times that even under supersaturated conditions, condensation does not occur. Mauritsen et al. (2011) estimated a threshold of 10–16 CCN per cm3 as a minimum to sustain clouds. As a result of these low concentrations, Arctic clouds and fogs are, therefore, sensitive to changes in particle concentration available for cloud droplet activation. There are a number of potential particle sources within the high Arctic during the summer: aerosols can be advected from the marginal ice zone (Bigg & Leck, 2001; Heintzenberg et al., 2006; Leck & Svensson, 2015); they can be transported from distance sources, such as marine and continental sources, although these are less important in the summer (Chang, Leck, et al., 2011; Schmale et al., 2022; Stohl et al., 2016); lastly, they can be generated locally from the open leads and within the pack ice (Held et al., 2011; Leck & Bigg, 2005; Orellana et al., 2011) or from blowing snow on the sea ice (Frey et al., 2020; Yang et al., 2008). Particles emitted directly from the open leads consist mainly of sea spray residuals (Leck et al., 2002), which are a mixture of ionic salts, like NaCl, and various biologically produced organic compounds (Leck et al., 2002; Leck & Svensson, 2015), including hygroscopic gel-like polymers around the refreezing period in the fall (Bigg et al., 2004; Hamacher-Barth et al., 2016; Orellana et al., 2011). These polymer structures are thought to degrade in sunlight into Aitken mode particles (smaller than 40 nm diameter) that can act as condensation nuclei for sulfuric acid (Lawler et al., 2021; Leck & Bigg, 2005). Finally, secondary aerosols can also be produced locally as a result of reactions between trace gases (e.g., sulfuric acid or iodic acid) and contribute to cloud formation in the atmosphere (Baccarini et al., 2020; Beck et al., 2021; Chang, Sjostedt, et al., 2011; Siegel et al., 2021).

Particle growth through water uptake and activation into a droplet can be estimated using the semi-empirical κ-Köhler theory (Köhler, 1936; Petters & Kreidenweis, 2007). It describes the water vapor supersaturation (SS) over an aqueous droplet based on its size and composition:

$$SS(D_{wet}) = \frac{D_{wet}^3 - D_{dry}^3}{D_{wet}^3 - D_{dry}^3(1-\kappa)} exp\left(\frac{4\sigma M_w}{\rho_w R T D_{wet}}\right) - 1 \quad (1)$$

where D_{wet} is the droplet diameter, D_{dry} is the dry particle diameter, M_w is the molecular weight of water (0.01802 kg mol^{-1}), σ is the surface tension of the droplet, assumed here to be that of pure water (0.072 N m^{-1}), R is the ideal gas constant, and T is the ambient temperature. The hygroscopicity parameter κ is compound- and mixture-specific and ranges from 0 for insoluble compounds such as soot (Weingartner et al., 1997) to 1.5 for very hygrophilic compounds such as pure sodium chloride (Zieger et al., 2017). While the hygroscopicity of single compounds and simple mixtures, such as sodium chloride and sulfuric acid, have been well explored (Schmale et al., 2018; Siegel et al., 2022; Svenningsson et al., 2006; Zieger et al., 2017), knowledge of ambient Arctic aerosol hygroscopicity still suffers from a deficit in measurements and modeling gaps (Schmale et al., 2021), since the aerosol sources, and therefore composition and size, are still poorly characterized.

Here we present observations of ambient aerosol and their hygroscopicity in and out of cloud events during the Arctic Ocean 2018 expedition (AO18). We investigated the droplet formation during high and low CCN concentration events, in relation to the limit described by Mauritsen et al. (2011), in the days before and after the re-freezing period (see Vüllers et al., 2021 for meteorological details). The role of Aitken mode particles in cloud droplet formation and lifetime will also be discussed. Section 2 presents the methods that were employed in this study, Section 3 details the results and includes some discussion on unexpected findings, and Section 4 summarizes our results and implications.

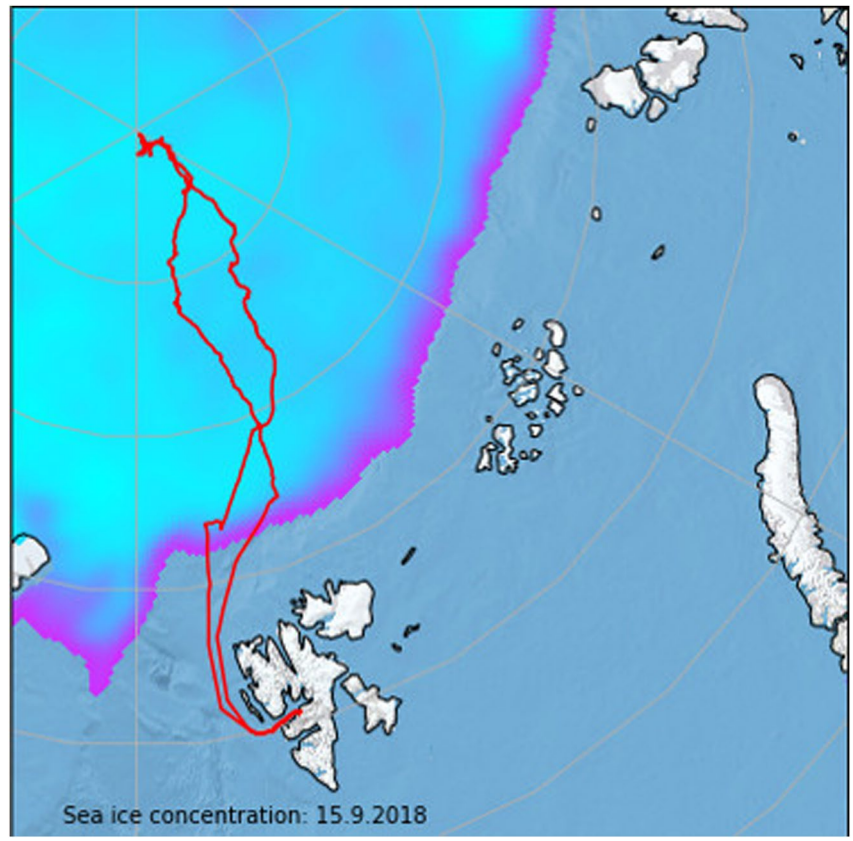

Figure 1. Ship track of the AO18 expedition (red), with sea ice concentration as of 15 September 2018 (bright blue and purple gradient; Spreen et al., 2008).

2. Methods

2.1. Expedition

The data presented in this paper were collected during the AO18, a joint United States-Swedish research cruise on board Swedish icebreaker (I/B) *Oden*. As shown on Figure 1, the ship departed from Longyearbyen, Svalbard (78.22°N, 15.65°E) on 1 August 2018 and headed northward around the island to arrive within the geographic North Pole (89.89°N, 38.04°E) on 12 August 2018. I/B *Oden* was moored to an ice floe of approximately 1 km^2 on 13 August 2018 (referred to as the Drift station), after which the ship headed back south starting on 14 September 2018. Two stations were conducted at the marginal ice zone, for a duration of 24 hr each, on 3 August (82.15°N, 9.97°E) and 19 September (82.28°N, 19.83°E) (more details in Leck et al., 2019).

2.2. Sample Inlets

2.2.1. Whole-Air Inlet

The whole air inlet was designed to sample interstitial aerosol and cloud particles up to ~40 μm diameter (following guidelines for whole-air aerosol sampling in extreme environments: WMO/GAW (2016); Wiedensohler et al. (2013)). It had a 7.6 cm outer diameter, a length of 4 m, and was installed on the container roof at a 45° angle, on the 4th deck on the ship at approximately 21 m above sea level. The inlet sampled a total of 90 L min^{-1} and the flow was heated to approximately 40°C to dry the particles, which can in some cases also slightly evaporate semi-volatile compounds. A hygrometer (Hytelog-USB, B + B Sensors, Germany) measured relative humidity at the end of the whole-air inlet, which was 12.1 ± 2.3% during the expedition.

2.2.2. Residual Inlet

A Ground-based Counterflow Virtual Impactor (GCVI; Brechtel Manufacturing Inc., USA, Model 1205) mounted on top of the laboratory container sampled only cloud droplets larger than 7.8 ± 1.0 μm in aerodynamic

diameter with a calculated enrichment factor of 6.4 ± 0.2. The cut size was established using a counterflow of 3 L min^{-1} and an added flow of 18 L min^{-1}. Droplets were dried within the GCVI before being measured by the aerosol instruments. To avoid interruptions in filter sampling, the GCVI was manually switched on when the visibility was <1 km and no precipitation was observed. When the GCVI was switched off, ambient air was sampled through the inlet just as the whole-air inlet. Further details on the operations of the GCVI for this study can be found in Karlsson et al. (2022).

2.3. Instruments

The particle number size distributions in the electrical mobility diameter (Dp) range of 10–921 nm, used for calculations of the total particle number concentration, were measured by differential mobility particle sizers (DMPSs) behind each inlet. The DMPSs behind the GCVI inlet consisted of a custom-built Vienna-type differential mobility analyzer (DMA) and a condensation particle counter (CPC; TSI, Model 3010). The DMPSs behind the whole-air inlet also consisted of a Vienna-type DMA and was connected to a mixing condensation particle counter (MCPC; Brechtel, Model 1702). Parallel to these instruments, an additional CPC and MCPC measured the total concentration of particles in the two inlets. The two DMPSs were calibrated using an aqueous suspension of 100 and 300 nm diameter polystyrene latex beads before and after the expedition. Size distributions were corrected for impaction, diffusion, and sedimentation losses following von der Weiden et al. (2009), and multiple charging following Wiedensohler (1988). Details on the correction and a comparison between both DMPSs systems, which very closely agreed, during non-cloudy periods can be found in Karlsson et al. (2022).

Each inlet also had a cloud condensation nuclei counter (CCNC, Droplet Measurement Technologies, CCN-100) that measured the number of ambient aerosol particles that activated into droplets at known supersaturations and recorded droplet size distributions in the range of 0.75–10 μm every second. They sampled with a sample flow of 0.05 L min^{-1} and a sheath flow of 0.45 L min^{-1}, for a total flow of 0.50 L min^{-1}. Each CCNC was calibrated using size-resolved ammonium sulfate particles with an assumed κ value of 0.6 for five different water vapor SS settings of nominal values 0.1%, 0.2%, 0.3%, 0.5% and 1.0%. Based on the calibration method described by Rose et al. (2008), these supersaturation settings were calculated to be 0.16%, 0.28%, 0.37%, 0.53%, and 0.89% for the CCNC behind the whole air inlet, and 0.18, 0.28, 0.39, 0.55, 0.96% for the CCNC on the residual inlet. During ambient measurements, the instrument cycled through the five supersaturation settings, 20 min at the first setting and 10 min at each of the other four, for a total time of 1 hr for one full cycle. For this analysis, the average concentration of the last 8 min at each setting was used, to allow the supersaturation to stabilize.

To maximize the sampling time, that is, to exclude contamination from the ship and from on ice activities, it was required that the inlets were facing upwind. In addition, a quality control was performed to remove suspected pollution and suspicious outliers from the measurements. The polluted data points were removed using the same method as in Karlsson et al. (2022). The flag was based on 1-s resolution particle number concentration from the MCPC behind the whole-air inlet. When the MCPC concentration range in a 30-s period exceeded 50 cm^{-3} as well as the mean absolute concentration over a 6-hr period centered on the same point, the data point was considered contaminated and removed. Any particle number concentration greater than 10^4 cm^{-3} was also removed. This was primarily to remove rapid concentration changes that occurred when a temporary source of pollution (e.g., from ship or helicopter exhaust) reached the sampling inlets, without removing noisy low-concentration data points. Overall, approximately 13% of the data points during the period at the drift station were considered polluted using this method. This pollution flag was applied to both sampling lines. In addition, the calibration periods were manually removed.

The liquid water content (LWC) and the effective radius (r_{eff}) of the cloud particles were measured by a particulate volume monitor (PVM; Gerber Scientific Inc., USA, Model PVM-100) installed on top of the laboratory container (approx. 20 m above sea level). Standard calibration procedures were performed, following the manufacturer's recommendations, and additional deviations were corrected by subtracting the signal present during clear (high-visibility) periods. To estimate the LWC limit of detection we have used the standard deviation of 10-min average values during high visibility (>15 km) and this was estimated to be 0.003 g m^{-3}. The ambient droplet number concentration (N_D) was estimated using the following formula:

$$N_D = \frac{3\,LWC}{4\pi\rho\,r_{eff}{}^3} \quad (2)$$

where ρ was assumed to be 1000 kg m^{-3}.

Temperature, wind and ship position data were recorded by the ship's navigation and meteorological systems (Prytherch & Tjernström, 2020). The meteorological conditions during the AO18 expedition are described in detail by Vüllers et al. (2021). The visibility data used in this paper were measured by the visibility sensor (Belfort Instrument, USA, Model 6400) integrated with the GCVI, using extinction at 880 nm and reported in a range of 0–50 km.

2.4. Activation Diameter and Hygroscopicity Calculations

The activation diameter (D_{act}) at each timestep and each inlet was calculated assuming an internally mixed aerosol based on previous observations in remote oceanic environments (Swietlicki et al., 2000). As a consequence, we assume that particles activated in descending order of diameter despite differences in hygroscopicity across the size spectrum. This calculation was performed by integrating the DMPS's size distribution downward until the total concentration of CCN measured by the CCNC at a given SS was reached. Following κ-Köhler theory, D_{act} was used with the SS to determine the hygroscopicity parameter (κ) (Petters & Kreidenweis, 2007) using the following equation:

$$\kappa = \frac{4}{ln^2(SS+1)}\left(\frac{4M_w\sigma}{3RT\rho_w D_{act}}\right)^3 \quad (3)$$

where SS is the set supersaturation, and D_{act} is the activation particle diameter determined from the CCNC measurements at each 10-min time step.

For individual events, κ was calculated from the averaged hourly κ values unless one or more of the values for a given SS were out of range (>1.2), in which case the κ was calculated based on the average D_{act} of the event for that SS.

It should be noted that the critical diameters associated with intermediate SS settings (0.28%, 0.37% and 0.53%) tended to fall in the intermodal range (generally around 70–100 nm) of the aerosol size distribution where lower number concentrations were measured. This had the effect of greatly amplifying the uncertainties associated with the calculated D_{act} and κ. For this reason, we focus on the highest and lowest SS settings (0.16% and 0.89%) for most of our analyses.

3. Results and Discussion

3.1. Overview

During the 32 days spent at the Drift station, the total ambient aerosol concentration larger than 10 nm diameter typically ranged between 19 and 116 cm^{-3} (25th and 75th percentile). Concentrations below 100 cm^{-3} occurred 73% of the time. The size distributions were generally bimodal (see Figure 2a), with an Aitken mode centered around 40 nm and an accumulation mode centered around 200 nm in diameter. The data were split into two based on the surface water freeze up, which started around August 28 (details in Vüllers et al., 2021). These two periods will be referred to as the pre-freeze and post-freeze periods, which differentiates the local open water-air interface from the sea ice-air interface. We expect microphysical differences between these two periods due to changes in influence from local marine biology as the season transitioned and blocked their pathway to the air. As discussed in Karlsson et al. (2022), 5-day back-trajectory analyses showed that on average, the source regions (ice, ocean, land) of the air sampled at the icebreaker did not change significantly before and after the freeze-up, so differences observed in the aerosol composition and size distribution between the two periods would be attributable to local and regional aerosol sources only.

3.1.1. Pre-Freeze Period (August 14–28)

Aerosol concentrations were very low during the week just before the freeze-up (August 20–27), often dropping below 10 per cm^3 (Figure S3 in Supporting Information S1). There was at least one event where the low concentrations seemed to limit droplet formation until the concentrations increased (see Section 3.2.2). The near-surface temperature was mostly between 0 and -2°C, with brief cooler periods of less than 2 days (Vüllers et al., 2021). As shown in Figure 2a, D_{act} for the highest and lowest SS tends to reflect the Aitken and accumulation modes,

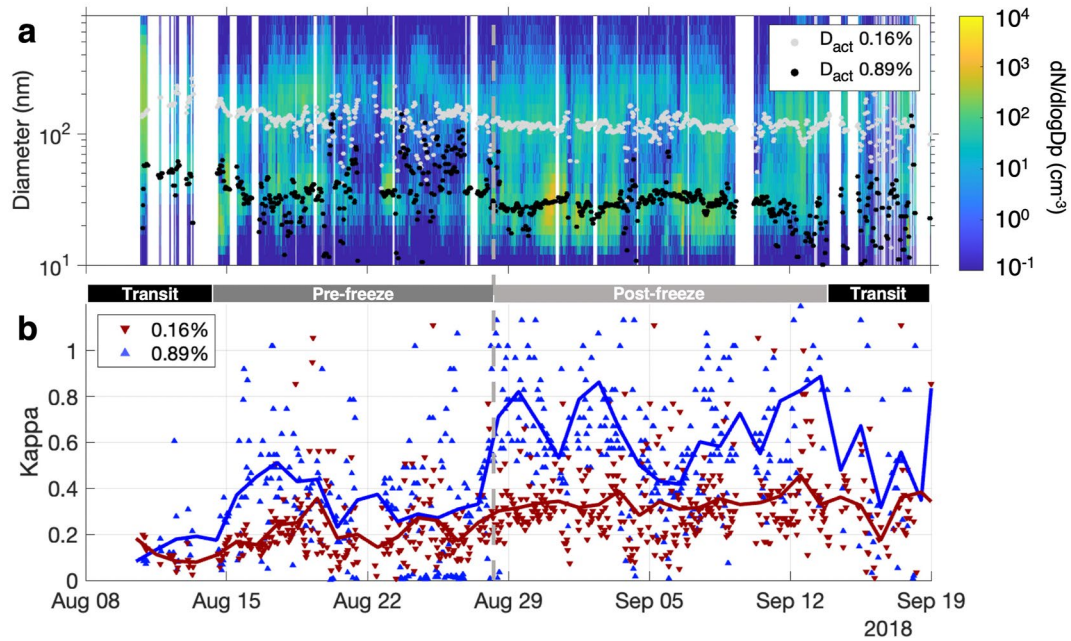

Figure 2. Whole-air time series of (a) the log-scaled number size-distribution and activation diameter for the lowest (gray points) and highest (black points) supersaturation settings, (b) hourly kappa values at the lowest and highest supersaturation (markers) and average daily kappa values at the highest and lowest supersaturations (full line). The gray vertical dashed line indicates the freeze-up time, and the different periods of the expedition covered by the time series are indicated between panels (a) and (b). The same figure, including the intermediate supersaturations in panel (b), is available as Figure S1 in Supporting Information S1.

respectively. The calculated κ for this period generally ranged between 0.1 and 0.3 at SS = 0.16% and 0.2–0.5 at SS = 0.89% (Figure 2b and Figure S2b in Supporting Information S1). The hygroscopicity values calculated for the accumulation mode during this period are relatively consistent with other high Arctic summer studies (0.08–0.21, Chang et al., 2022, 0.33 ± 0.13, Martin et al., 2011, 0.1–0.4, Leck & Svensson, 2015), and support that the accumulation mode particles had a significant organic fraction, as shown in Karlsson et al. (2022), potentially from the condensation of organic vapors.

In comparison, the Aitken mode was more hygroscopic during this period, possibly due to the presence of sulfate and sodium (see Lawler et al., 2021). This trend is the opposite of previous Central Arctic studies in summertime, where Aitken mode particles were inferred to be less hygroscopic than accumulation mode particles from CCN measurements (Leck & Svensson, 2015; Martin et al., 2011) as well as in the Canadian Arctic (Chang et al., 2022). Although more influenced by open waters and continental sources with varying degrees of pollution (see Karl et al., 2019), values reported from the Zeppelin research station in late summer (~0.57, Zieger et al., 2010, p. 0.3–0.5, Zábori et al., 2015) are sometimes similar to our values, although it should be noted that the former study at Zeppelin was measured under subsaturated conditions. However, values reported from the Canadian Arctic (0.04–0.08, Chang et al., 2022) are much lower. These past studies illustrate the variability of aerosol hygroscopicity across the Arctic region, depending on the proximity to land and local biodiversity. Higher hygroscopicity in the Aitken mode compared to the accumulation mode is not unheard of, but to our knowledge, has only been previously reported in highly polluted environments (e.g., Chen et al., 2022). However, Lawler et al. (2021) showed a strong presence of sodium and potentially hygroscopic sodium-bonded polysaccharides in the Aitken mode, which could in part explain the high hygroscopicity shown here.

3.1.2. Post-Freeze Period (August 28—September 14)

The particles were statistically more hygroscopic at all SS during the post-freeze period (Figure 2b and Figure S2b in Supporting Information S1), especially at the highest SS, with 24-hr mean values occasionally reaching $\kappa = 0.85 \pm 0.13$ around August 28–30 and September 2–3 (Figure 2b). This suggests that the Aitken-mode particles were more hygroscopic following the freeze-up, either because they were composed of more hygroscopic compounds, or due to the presence of surface-active compounds, as discussed below. Baccarini et al. (2020)

Table 1
Atmospheric and Whole-Air Inlet (WAI) Aerosol Characteristics Before the Freezing Period (Pre-Freeze) and After the Freezing Period (Post-Freeze)

Period	Start (UTC)	End (UTC)	Median temp (°C)	Time with vis <1 km (%)	Aitken ratio (WAI)	Median act ratio (WAI)		Median kappa (WAI)	
						SS = 0.16%	SS = 0.89%	SS = 0.16%	SS = 0.89%
Pre-freeze	13 Aug 19:20	28 Aug 12:00	−1.2	16.9	0.57	0.24	0.67	0.18 ± 0.15	0.34 ± 0.27
Post-freeze	28 Aug 12:00	14 Sep 21:00	−4.3	8.5	0.68	0.19	0.61	0.30 ± 0.17	0.57 ± 0.29

Note. Both cloudy and clear conditions are included. Uncertainties on Kappa values represent one standard deviation.

showed that the post-freeze period was characterized by higher iodine emission leading to new particle formation events and an increase in the ultrafine (diameter <15 nm) particle concentration by about a factor of 10. Lawler et al. (2021) also found a large increase in the Aitken mode particulate iodine concentration (about a factor of 6), although iodine only contributed to a few percent of the total Aitken mode mass, so it cannot explain the higher hygroscopicity inferred from the CCNC measurements. Sulfate, instead, was one of the main constituents of Aitken mode particles and increased by 48% after the freeze-up (in relative terms) (Lawler et al., 2021), which would have contributed to a higher hygroscopicity. Sodium was also found in significant amounts in the Aitken mode particles, which could also potentially contribute to the increase in hygroscopicity. However, not only did sodium concentration not increase around freeze-up, but also TEM image analyses from the Arctic Summer Cloud Ocean Study in 2008 in the same region and season has shown that sodium is organically bonded (Hamacher-Barth et al., 2016), which would potentially limit its hygroscopicity. Using data from the last 9 days of our expedition (September 11-19), Siegel et al. (2022) conducted an aerosol-CCN closure study and observed good general agreement between predicted and observed CCN concentrations based on chemical analysis and aerosol size distribution, with overall uncertainties below 20%. However, they also inferred high κ values for the Aitken mode which could not be explained with the chemical analysis.

Aitken mode particles were predominant in the second half of the drift, especially in the first week of the post-freeze period (Figure 2a). Despite the higher κ values, this period of higher total particle number concentration led to a slightly smaller fraction of particles larger than 10 nm activating into droplets at the highest supersaturation (SS = 0.89%) in the post-freeze period compared to the pre-freeze period (Table 1). This is likely to have been a result of the relatively more numerous Aitken mode particles that were too small to activate. κ values derived from the lowest supersaturation (SS = 0.16%) were also higher after the freeze-up, with a maximum of around $\kappa = 0.4$ around September 5, suggesting that overall, all the particles were more hygroscopic in the second part of the drift.

One possible explanation for the higher κ calculated for the Aitken mode (SS = 0.89%; $\kappa = 0.57 \pm 0.29$) compared to the pre-freeze period is the presence of surface active compounds, which would violate the assumption in Equation 3 that the surface tension remains that of pure water during droplet growth. Siegel et al. (2021) found that aerosols present during the last 9 days of the expedition contained long-chain fatty acids, which are insoluble in water but could theoretically reduce the surface tension of the droplets and therefore increase CCN activation (Hamacher-Barth et al., 2016; Lawler et al., 2021; Leck & Svensson, 2015; Orellana et al., 2011; Ovadnevaite et al., 2017).

3.2. Fog Events

We identified eight cases (detailed in Table 2 and Table S1 in Supporting Information S1) in which visibility dropped below 1 km for at least two consecutive hours, with at most one interruption of less than 30 min, and the GCVI was turned on. These will be referred to as fog due to our proximity to the surface and the visibility criteria. However, it should be recognized that these findings could also be relevant for Arctic clouds, which can be thin and near the surface. From the eight events, one of them occurred near the end of the transit to the North Pole, four of them in the pre-freeze period, and three in the post-freeze period. One significant fog event occurred during the week following the freeze-up (August 29–September 5), but could not be fully analyzed due to an issue with the CCNC (see SI for details). The following subsections describe the microphysics around the formation and persistence of these events.

It should be noted that κ values have high uncertainties because of the multiple uncertainties that propagate into their calculation. The two main sources of uncertainties are in the supersaturation of the CCNC, and in the particle counts that are used to determine the effective activation diameter from the size distribution. Assuming

Table 2
Summary of the Eight Main Fog Events for Whole-Air Inlet (WAI) and Residuals (Res)

Start	End	N_p WAI (cm^{-3})	N_p Res. (cm^{-3})	Aitken frac. WAI	Accum frac. WAI	r_{eff} (μm)	75th p r_{eff} (μm)	75th p LWC (g m^{-3})	Temp. (°C)	D_{act} WAI 0.16% (nm)	κ WAI (0.16%)	κ WAI (0.89%)	κ Res. (0.18%)	κ Res. (0.96%)
Aug 10 19:54	Aug 10 23:30	231	49	0.18	0.82	5.8	6.9	0.029	−0.2	139	0.18 ± 0.02	0.09 ± 0.01	0.36 ± 0.48	[c]
Aug 18 15:42	Aug 18 22:37	66	13	0.36	0.64	7.3	7.5	0.057	−0.1	134	0.21 ± 0.07	0.33 ± 0.12	0.24 ± 0.10	[c]
Aug 22 17:42	Aug 22 20:15	42	23	0.56	0.44	9.0	9.3	0.064	−0.3	141	0.19 ± 0.09	0.38 ± 0.06	0.11 ± 0.02	0.17[a] ± 0.13
Aug 24 15:42	Aug 24 18:49	9	3	0.12	0.88	8.4	8.5	0.021	−0.6	87	0.22 ± 0.02	0.49[d]	0.18 ± 0.08	[c]
Aug 26 17:42	Aug 26 20:40	13	6	0.48	0.52	5.4	8.1	0.013	−1.5	142	0.17 ± 0.01	0.02 ± 0.01	0.16[d]	[c]
Sep 06 07:54	Sep 06 11:40	63	12	0.93	0.07	9.3	11.0	0.101	−7.9	143	0.23 ± 0.14	0.42 ± 0.05	0.01 ± 0.01	0.16 ± 0.11
Sep 10 16:42	Sep 10 19:40	25	6	0.78	0.22	8.6	9.0	0.047	−11.8	142	0.17 [d]	0.69 ± 0.24	0.25 ± 0.18	0.86[b] ±0.67
Sep 11 13:42	Sep 11 18:00	27	6	0.43	0.57	6.8	6.9	0.067	−9.4	118	0.30 ± 0.06	0.36 ± 0.02	0.29 ± 0.26	0.30 ± 0.14

Note. Here are listed the mean (or otherwise noted) values of particle number concentration (N_p), number fraction of Aitken mode particles (10–80 nm diameter) and accumulation mode particles (80–500 nm diameter), mean and 75th percentile effective radius (r_{eff}), 75th percentile liquid water content (LWC), mean temperature, estimated activation diameter (D_{act}) and hygroscopicity parameter κ. Uncertainty on **κ** represents 1 standard deviation.
[a]κ for SS = 0.55%. [b]κ for SS = 0.28%. [c]κ not representative due to constant D_{act} at many SS. [d]Too few valid data points to calculate a standard deviation.

an uncertainty of 0.01% supersaturation and 1 nm uncertainty in the sizing of the DMPSs would result in an uncertainty in the κ of 7%–13%. Assuming an uncertainty of 5% in the CCN concentration would result in an uncertainty in the κ of ∼15%.

3.2.1. Size Distribution of Droplet Residuals and Activation Diameter

Consistent with the results of the entire study presented in Section 3.1, which includes clear periods, during fog periods, the smaller particles were more hygroscopic than the larger ones in both the whole-air and GCVI residual lines (Table 2). Figure 3 shows the size distribution of the residuals and the estimated D_{act} at each SS. In five out of the eight events (10, 18, 22, 26 August, and 10 September), the Aitken mode of the residual particles did not activate in the CCNC, even at the highest SS of 0.96% (further discussion in Section 3.2.3), and the estimated D_{act} remained larger than the entire Aitken mode for all SS. This sometimes led to a D_{act} that was relatively stable over multiple SS, which is especially apparent for August 10, 18, 22, 24 and September 10. In such cases, the lowest SS with that D_{act} was used to calculate the κ value (see Figure S5 in Supporting Information S1). This is reflected in the κ values presented for the residual particles at SS of 0.96% in Table 2. For the case of August 26, D_{act} increased with an increasing SS, which could be due either to (1) the chemical speciation of the residuals or their size distribution varying significantly during the event, or (2) a similar case as the five previously mentioned events, but the number concentrations were too low and resulted in large uncertainties in the calculations. It should be noted that this event had the least dense fog overall, including 24 min of visibility >1 km, adding a large variability within the hourly CCNC scan. For hypothesis (1), since trace gases (CO, CH_4) were relatively stable (changes of less than 4 ppb(v), see Figure S7e in Supporting Information S1) during the event, we assume the air mass remained the same and that the particle chemical composition did not vary significantly. However, aqueous chemistry in the evolving droplets could have potentially altered the composition of the aerosols throughout the event. In contrast, the event of September 6 showed an expected result where D_{act} monotonically decreased as SS increased (Figure 3f).

3.2.2. CCN-Limited Regime

During ASCOS performed in the central Arctic Ocean in 2008, Mauritsen et al. (2011) observed that clouds did not form during a period of low particle concentrations and calculated that at concentrations less than 10 to

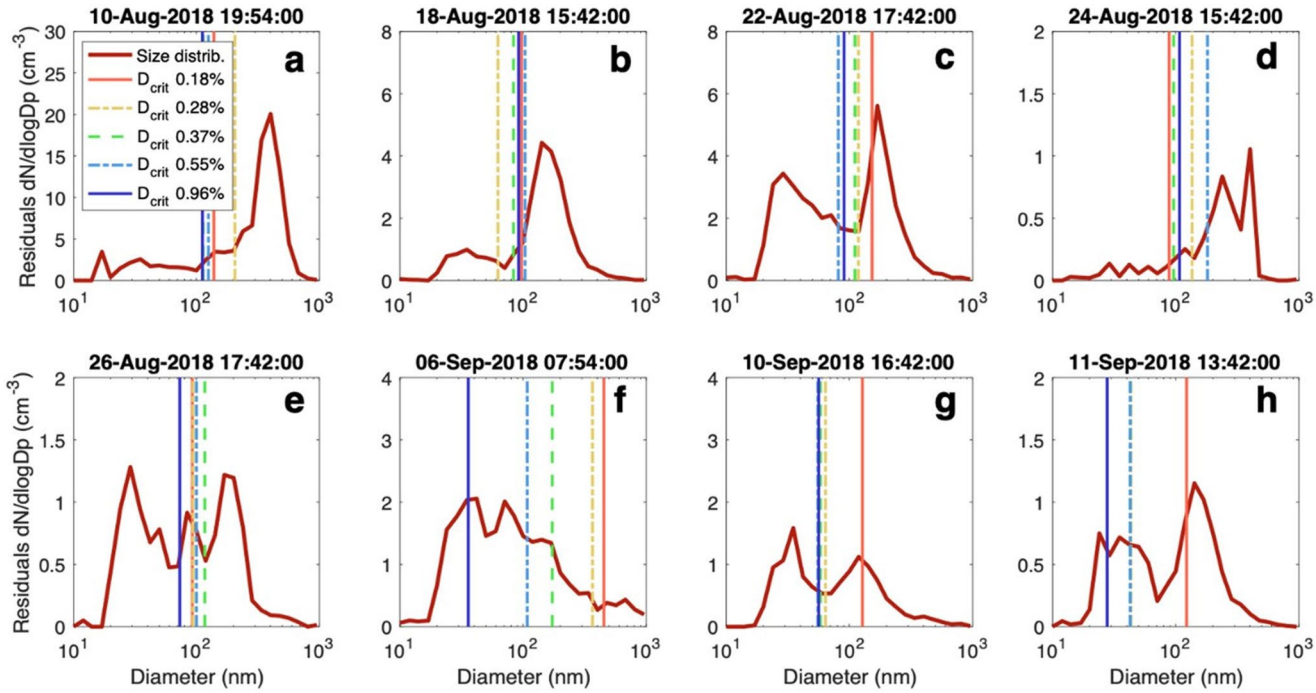

Figure 3. Mean residuals size distribution (dark red line) for each of the eight events starting at the time shown above each panel, and mean activation diameter (D_{act}) at each supersaturation (vertical lines, color-coded in panel a). Residual concentrations are corrected for the CVI enrichment factor to reflect their actual abundance in the fog. Increasing D_{act} with supersaturation is discussed in Section 3.2.1.

16 CCN per cm^3, assming sufficient supersaturation, activated droplets can often rapidly grow large enough to precipitate since there are insufficient particles to compete for the available water vapor and limit their growth, thus reducing the lifetime of the cloud. Clouds limited by CCN were also observed by Leck and Bigg (1999), and Lohmann and Leck (2005) in the central Arctic, as well as Leaitch et al. (2016) in the Canadian Arctic summer and modeled by Dionne et al. (2020). During AO18, the near-surface air was very moist, generally close to 100% relative humidity with frequent supersaturation with respect to water before the freeze-up, and with respect to ice before and after the freeze-up (Vüllers et al., 2021). Therefore, the presence of water vapor was generally favorable for cloud formation. The events on 22, 24, 26 August and 6, 10 September were identified as having very low particle concentrations and potentially CCN-limited (Figures 4c–4g). These events met at least one of the following criteria during the events or in the three hours preceding them: (1) the total particle concentration was below 10 per cm^3 or (2) the total concentration of the accumulation mode particles was below 5 per cm^3. The 22 August event is the most likely to have been CCN-limited, since the fog formation coincided with when the concentration of particles larger than 10 nm in diameter increased from <10 to >30 per cm^3 and the concentration of particles larger than 80 nm in diameter increased from <5 to ∼20 per cm^3, presumably sufficiently high for the droplets to be observed (Figure 4c). This change may have been caused by a new air mass moving in. Although the local temperature and wind speed and direction did not change (see Figure S6a in Supporting Information S1), O_3 and CH_4 showed changes of 10–30 ppb(v) (Figure S7 in Supporting Information S1), which generally coincided with the increase in aerosol loading. Local pollution was ruled out as it would have caused rapid and intense variations in the O_3 and CO time series (Beck et al., 2022) and our observations are consistent with the possibility that the increase in ambient particle concentration triggered fog formation. The fog events on August 26 and September 10 were also characterized by very low pre-fog concentrations of particles larger than 80 nm in diameter (<5 per cm^3), but it is less clear whether the increase in CCN triggered fog formation, since the increase was smaller but perhaps just large enough to form and maintain the cloud. Interestingly, the event on August 24 resulted in a continuous fog with visibility between 500 and 1000 m (Figure S6b in Supporting Information S1), despite the residual particle concentrations remaining below 10 particles per cm^3 for almost the entire three-hour duration (Figure 4d). This was possibly due to the dominance of accumulation mode particles (Figure 3d, Figure S4d in Supporting Information S1) that would have had to compete for any available water vapor and therefore prevented them from growing large enough to fall out. In contrast, the 6 September event was dominated by Aitken mode

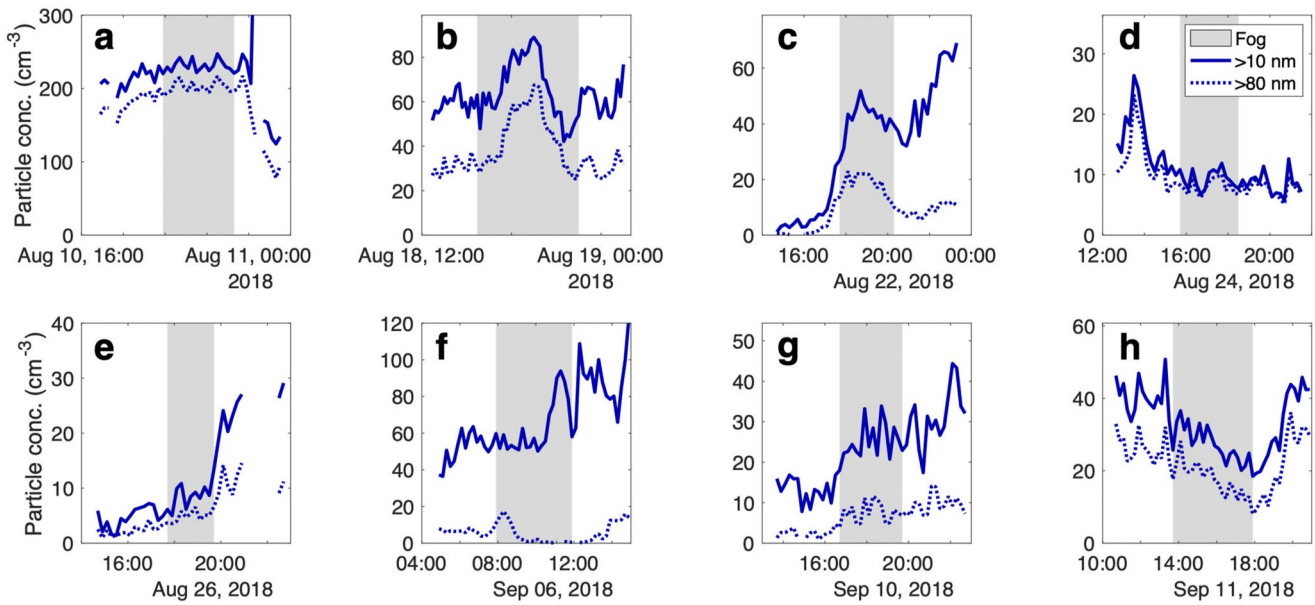

Figure 4. Particle concentrations >10 nm from the whole air inlet (WAI) for each of the eight significant fog events (a through h) at or near the north pole. The concentration of particles larger than 80 nm in the whole air inlet is shown in the dotted line, and the fog periods are indicated by a gray shading.

particles with a nearly absent accumulation mode (Figure S4f in Supporting Information S1), providing evidence that Aitken mode particles can participate in maintaining a cloud when the accumulation mode is absent, as suggested by the simulations conducted by Bulatovic et al. (2021) and inferred by Karlsson et al. (2022) for Arctic low clouds. Similar results were presented in Koike et al. (2019) and Karlsson et al. (2021), although they may not have been representative for the high Arctic pack ice. An increase in the Aitken mode aerosol concentration was also measured in the latter part of the event, consistent with the results reported by Heintzenberg et al. (2006). The appearance of these particles also coincided with an increase in methane concentration (Figure S7f in Supporting Information S1), suggesting that the aerosol increase was associated with a change in the characteristics of the air mass.

With the low CCN concentrations during the identified CCN-limited events, we would expect these droplets to be larger than those in other events where the CCN concentrations were higher because there would be less competition for water-vapor condensation. Figure 5 shows the r_{eff} and LWC for all low visibility (<1 km) data points in gray and the larger colored points represent the median of each of these parameters for individual fog events. Note that these colored points are only statistical indicators of the droplet properties during fog events and do not represent a specific r_{eff} and LWC combination at any particular point in time. The red points show that the resulting r_{eff} for a given LWC is higher in four of the five CCN-limited cases compared to the events in which higher particle concentrations were present, consistent with our expectations. The 25–75th percentile ranges also have minimal overlap, which supports that each group is statistically different. However, unlike the study by Mauritsen et al. (2011), this enhanced growth was not sufficient to precipitate the CCN fast enough to dissipate the cloud immediately. It is important to note that our events were relatively short (2–6 hr) compared to the hourly time resolution of their model and that at a lower time resolution it could have appeared as though the cloud dissipated instantly. It would be interesting to investigate additional cases that were so limited by the CCN that visibility would not have been reduced enough to be detected as fog, as one of the cases analyzed by Leck and Svensson (2015). However, the available condensable water was not yet analyzed so it is difficult to identify these cases at this point. Overall, these observations strongly suggest that very low CCN availability affected cloud formation, but also that clouds can form and persist, at least for a couple of hours, at lower aerosol concentrations that may have been previously thought to be too low to permit cloud formation.

3.2.3. Activation Ratio of Whole Air Particles Versus Cloud Residuals

Residuals of liquid cloud droplets are generally expected to have an activation ratio that is higher than that of the whole air particles, since they have already activated and were sampled as droplets by the GCVI inlet.

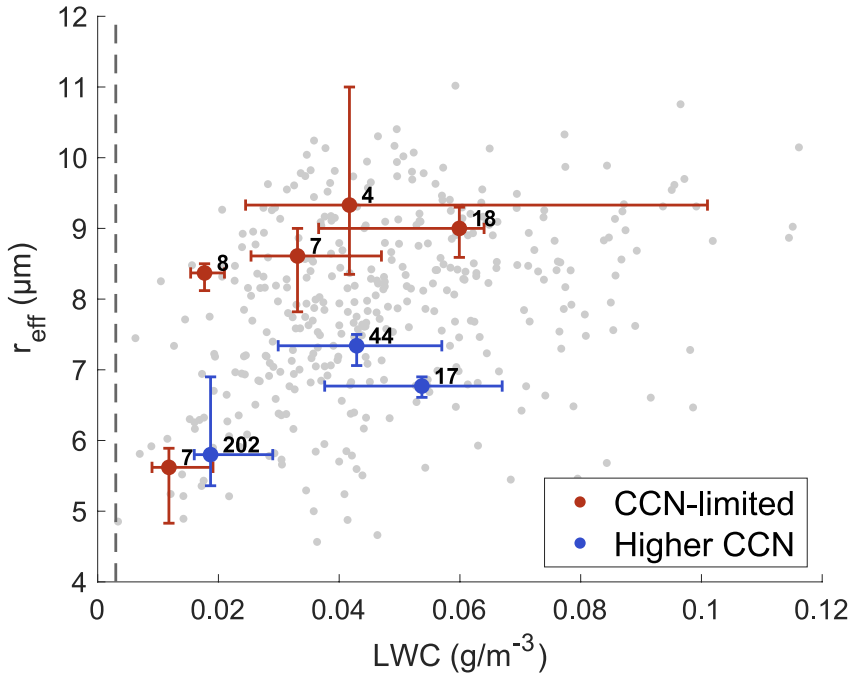

Figure 5. Effective radius (r_{eff}) against liquid water content (LWC) for all low-visibility (<1 km) data points (gray), events with CCN-limited concentration (red), and higher CCN concentration (blue). Event data points are median values of r_{eff} and LWC, and the 25th and 75th percentile ranges are shown with the error bars. Mean number concentration of particles larger than 80 nm are indicated to the right of each event point. The estimated limit of detection of LWC is indicated by the dashed line at LWC = 0.003 g m^{-3}.

Furthermore, aqueous processing in the droplets is generally oxidizing, involving volatile organic compounds, sulfur dioxide or dimethyl sulfide reacting with aqueous OH, forming sulfuric acid and methanesulfonic acid, which would be expected to increase hygroscopicity and cloud residual size further (Aljawhary et al., 2016; Barnes et al., 2006; Chen et al., 2018; Ervens et al., 2011). The observed activation ratios for the eight fog events are shown in Figure 6 behind the GCVI (blue line) and for the whole air particles (orange line). Only the event of 10 September consistently had higher activation ratios for the residual particles, with a higher κ for the residuals (0.34) compared to the κ for the whole air particles (0.24) at SS = 0.16–0.18 (Table 2). For all the other events, the high uncertainties render possible differences between the activation ratios difficult to discern, although the κ values are sometimes higher for the whole air particles (Table 2). In general, the activation ratio is limited by the non-activation of an Aitken mode present in both sampling lines. This is demonstrated for the residual particles in Figure 3, where only two of the six cases that included a significant Aitken mode present activated (i.e., D_{act} included the Aitken mode, panels f and h). Therefore, the activation ratios are often similar in the two lines despite a higher presence of hygroscopic components such as sulfate in the droplets (Karlsson et al., 2022). Since the Aitken mode is still present in the droplet residuals and therefore must have activated prior to sampling, possible explanations are that either (1) the peak SS at the onset of the cloud formation was often higher than 1%, which is within the possible range from model simulations presented in Bulatovic et al. (2021), or, more likely, (2) the water uptake on those particles is generally too slow for droplet activation to occur in the short residence time of the particles in the CCNC cloud chamber, as previously suggested by Leck and Svensson (2015), or (3) that the drying process evaporated not only water, but also a fraction of the solute, which would affect the residuals ability to reactivate into a droplet, as suggested by Rissler et al. (2023). The presence of an Aitken mode in the residuals is unlikely due to sampling artifacts by the GCVI, such as droplet break up, particle capture by wake effect, or ice crystal shattering, which start occurring at larger crystal diameters than those sampled in these events, as extensively discussed in Karlsson et al. (2021, 2022).

The activation ratio of the droplet residuals can be used to infer the ambient SS at which the cloud formed. Figure 6 shows that the activation ratio was sometimes high and constant at all SS behind the GCVI (August 10, 18, 24), suggesting that the ambient SS was lower than the lowest SS of the CCNC (0.18%). In other cases (September 6,

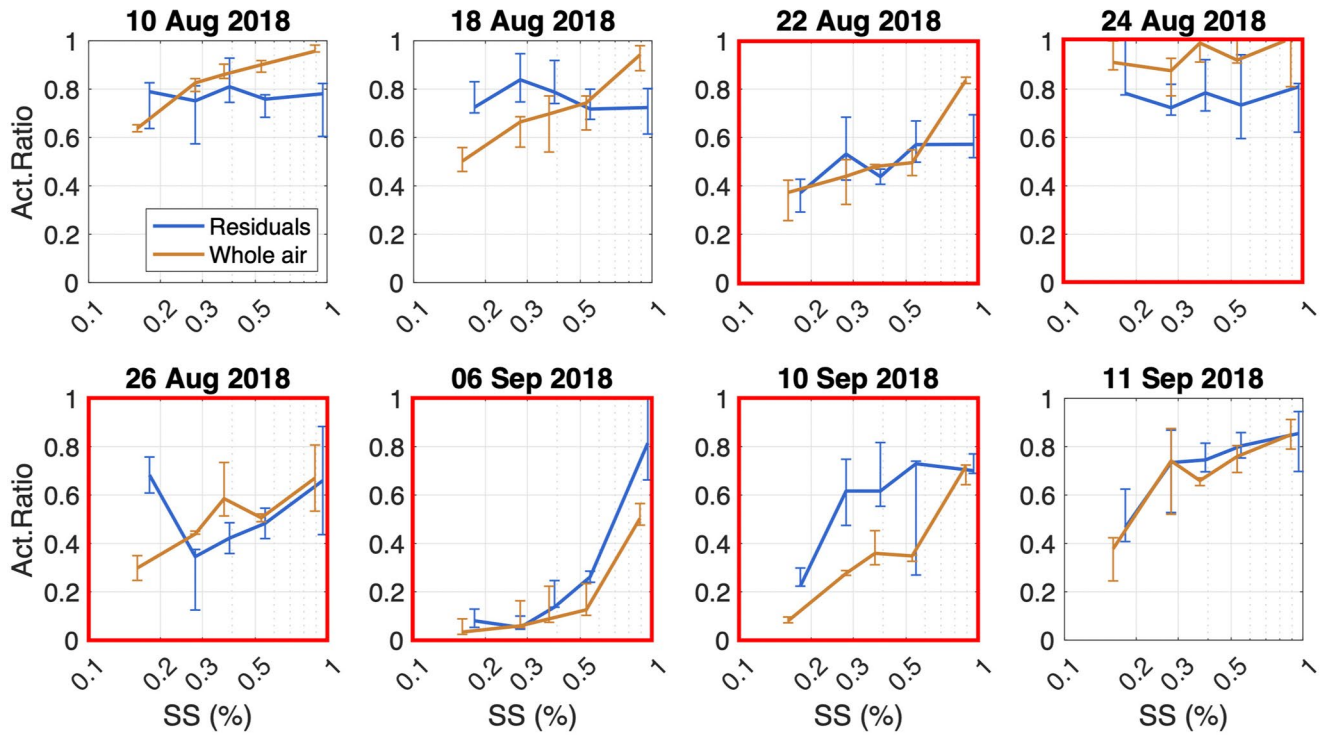

Figure 6. Mean activation ratios during each event, for the droplet residuals and whole air particles at five selected supersaturations. Title above each panel indicates the date on which the event occurred. Error bars indicate the 25th and 75th percentile range. Red frames indicate events that were considered CCN-limited.

10, 11), the activation ratio increased sharply between two SS. In these cases, the curve would suggest an ambient SS between 0.57% and 0.96% for September 6, and between 0.16% and 0.28% for September 10 and 11. For the case of August 22, which was likely CCN-limited, the activation ratio remained relatively low at all SS, suggesting that the droplets from that fog might have formed at ambient SS greater than the highest setting of the CCNC (0.96%). The lowest activation ratios behind the GCVI (August 18, 22, and September 10) occurred during events in which the Aitken mode made up a significant fraction of the droplet residuals (Figure 3). Past studies have shown that when accumulation mode particles are too scarce to take up the excess water vapor, Aitken mode particles can activate and maintain the cloud (Bigg & Leck, 2001; Bulatovic et al., 2021; Karlsson et al., 2021; Korhonen et al., 2008; Leck et al., 2002; Lohmann & Leck, 2005), which can lead to high peak supersaturation during the cloud formation potentially exceeding 1% (Bulatovic et al., 2021). A parcel model simulation using aerosol distributions from this expedition was also presented by Karlsson et al. (2022) who showed that, given high but not unheard of cooling rates, particles as small as 25 nm in diameter can be activated. Since the highest SS setting of the CCNC was 0.96% during our measurements, it is possible that it was simply not high enough to activate a fraction of the smallest residuals sampled. This can be observed in the September 6 event where the fog maintained itself despite a near-zero accumulation mode number concentration. Overall, we are still unable to explain why a larger fraction of those Aitken mode particles activated in the whole air compared to the residuals.

4. Conclusions

After almost 5 weeks moored at an ice floe near the North Pole around the refreezing period (28 August 2018), there were eight main cloud/fog events that could be analyzed for the purpose of this paper. Very low aerosol number concentrations were measured during the week preceding the freeze-up, and generally higher concentrations were measured after the freeze-up, but with smaller diameters. In some cases, fog events occurred when background particles larger than 10 nm in diameter were below 10 per cm^3, which is below the limit for cloud formation previously suggested in Mauritsen et al. (2011). In low-CCN concentration clouds, we observed droplets larger than those in the high-CCN concentration cases at equal LWC, consistent with a greater uptake of the available water on the fewer CCN available. Our results support the notion that Aitken mode particles can help sustain a cloud when accumulation mode particles are insufficient.

We found that while a larger fraction of the droplet residuals activated into droplets in the CCNC, greater activation was sometimes observed in the whole-air particles. It is likely that these cases can be attributed to the significant presence of non-activating or partially activating (at SS <1%) Aitken mode, present in the residuals. Even in the cases where a larger fraction of residuals reactivated under supersaturation, full reactivation was not reached at any of the tested supersaturations. Although alternative hypotheses, such as the dynamics of water uptake in the CCNC chamber, warrant further study, our results suggest that ambient supersaturation at cloud formation could have been >1%.

The calculated κ associated with the Aitken mode was greater than that of the accumulation mode, especially after the freeze-up. κ values were very high for the high Arctic region, ranging between 0.4 and 0.85 during the most hygroscopic period for SS = 0.89%. Peak hygroscopicity was observed during a new particle formation event discussed in Lawler et al. (2021) and Baccarini et al. (2020). The presence of hygroscopic organics and sodium in the Aitken mode, as shown in Lawler et al. (2021), could have contributed to some of the hygroscopicity. Xu et al. (2022) suggest that the Aitken mode is much more hygroscopic than current estimates at a global scale, mainly due to the presence of inorganic sea salt in particles down to 35 nm in diameter, although the relevance of their findings to the high Arctic where open water is limited is unknown. Finally, the presence of surface-active organics, such as insoluble long-chain fatty acids (Siegel et al., 2021) that could help droplet formation by lowering surface tension, could also explain the higher hygroscopicity observed. The presence of polysaccharides, potential surfactants, was also noted by Lawler et al. (2021) in an event occurring on Aug 30-31, shortly after the freeze-up. These compounds can also turn into hydrophilic gels if given time to slowly adsorb water, which have been hypothesized to promote cloud droplet formation (Orellana et al., 2021). In the end, despite a potential κ overestimation caused by surface activity, our results suggest that Aitken mode particles were very CCN-active in late summer and fall in the Central Arctic during the AO18.

Overall, our results suggest that, due to high hygroscopicity, cloud formation proceeded with lower aerosol number concentrations than were previously thought possible, but likely with shorter lifetimes. These tenuous clouds in the Arctic summer have been shown to result in net warming at the surface (Mauritsen et al., 2011), which necessitates an improved understanding of their formation, persistence, and dissipation so that their radiative effects can also be better understood. The mechanism of supersaturation generation during the events in our study likely also played an important role on the observed variability, although it remains unexplored at this time and warrants further study.

Data Availability Statement

The data of the Arctic Ocean 2018 expedition is available at the data centre of the Bolin Centre for Climate Research (https://bolin.su.se/data/oden-ao-2018-expedition-1; Leck et al., 2021). The aerosol data used in this study are found here: https://doi.org/10.17043/oden-ao-2018-aerosol-cvi-1; Karlsson et al., 2022) and the cloud condensation nuclei data are available here: https://doi.org/10.17043/oden-ao-2018-ccnc-1; Duplessis et al., 2023).

Acknowledgments
This work was supported by the Natural Sciences and Engineering Research Council of Canada (RGPIN-2014-05173); the Canadian Transatlantic Ocean System Science & Technology (TOSST) program; the Ocean Frontier Institute, through an award from the Canada First Research Excellence Fund; the Knut-and-Alice-Wallenberg Foundation within the ACAS project (Arctic Climate Across Scales, project no. 2016.0024); the Bolin Centre for Climate Research (RA2), the Swedish Research Council (VR Grants, 2018-05045, 2016-03518, and 2016-05100); the Swiss National Science Foundation (Grants 200021_169090 and 200021_188478); the Swiss Polar Institute; the BNP Paribas Swiss Foundation (Polar Access Fund 2018). J.S. holds the Ingvar Kamprad Chair for Extreme Environment Research, sponsored by Ferring Pharmaceuticals, and R.Y.-W.C. holds a Canada Research Chair, administered by the Natural Sciences and Engineering Research Council of Canada. We also thank John Prytherch and Michael Tjernström (Stockholm University, Sweden) for processing temperature and wind speed data. We are also grateful to Julika Zinke, Leif Bäcklin, Tabea Hennig, Ondrej Tesar, Nils Walberg, and Alexander Håkansson for their technical support. The Swedish Polar Research Secretariat (SPRS) provided access to the I/B *Oden* and logistical support in collaboration with the U.S. National Science Foundation. B.S. acknowledges SRA MERGE for creating a stimulating scientific community. We are grateful to the Co-Chief Scientist Patricia Matrai for planning, technical support, and coordination of AO2018, to the SPRS logistical staff and to I/B *Oden*'s Captain Mattias Peterson and his crew for expert field support. Last but not least, we would like to thank Fred Brechtel, Annica Ekman, Matthew Salter, and Michael Lawler for the valuable scientific discussions.

References

Aljawhary, D., Zhao, R., Lee, A. K. Y., Wang, C., & Abbatt, J. P. D. (2016). Kinetics, mechanism, and secondary organic aerosol yield of aqueous phase photo-oxidation of α-Pinene oxidation products. *Journal of Physical Chemistry A*, *120*(9), 1395–1407. https://doi.org/10.1021/acs.jpca.5b06237

Baccarini, A., Karlsson, L., Dommen, J., Duplessis, P., Vüllers, J., Brooks, I. M., et al. (2020). Frequent new particle formation over the high Arctic pack ice by enhanced iodine emissions. *Nature Communications*, *11*(1), 1–11. https://doi.org/10.1038/s41467-020-18551-0

Barnes, I., Hjorth, J., & Mihalapoulos, N. (2006). Dimethyl sulfide and dimethyl sulfoxide and their oxidation in the atmosphere. *Chemical Reviews*, *106*(3), 940–975. https://doi.org/10.1021/cr020529

Beck, I., Angot, H., Baccarini, A., Dada, L., Quéléver, L., Jokinen, T., et al. (2022). Automated identification of local contamination in remote atmospheric composition time series. *Atmospheric Measurement Techniques*, *15*(14), 4195–4224. https://doi.org/10.5194/amt-15-4195-2022

Beck, L. J., Sarnela, N., Junninen, H., Hoppe, C. J. M., Garmash, O., Bianchi, F., et al. (2021). Differing mechanisms of new particle formation at two arctic sites. *Geophysical Research Letters*, *48*(4), 1–11. https://doi.org/10.1029/2020GL091334

Bigg, E. K., & Leck, C. (2001). Cloud-active particles over the central Arctic Ocean were typically in the range -3 but of IFN ranged from the pack ice at the beginning of the expedition at the end. The differences with transport time from the ice edge were less marked. *Journal of Geophysical Research*, *106*(D23), 32155–32166.

Bigg, E. K., Leck, C., & Tranvik, L. (2004). Particulates of the surface microlayer of open water in the central Arctic Ocean in summer. *Marine Chemistry*, *91*(1–4), 131–141. https://doi.org/10.1016/j.marchem.2004.06.005

Bulatovic, I., Igel, A. L., Leck, C., Heintzenberg, J., Riipinen, I., & Ekman, A. M. L. (2021). The importance of Aitken mode aerosol particles for cloud sustenance in the summertime high Arctic-A simulation study supported by observational data. *Atmospheric Chemistry and Physics*, *21*(5), 3871–3897. https://doi.org/10.5194/acp-21-3871-2021

Chang, R. Y.-W., Abbatt, J. P. D., Boyer, M. C., Chaubey, J. P., & Collins, D. B. (2022). Characterizing the hygroscopicity of growing particles in the Canadian Arctic summer. *Atmospheric Chemistry and Physics*, *22*(12), 8059–8071. https://doi.org/10.5194/acp-22-8059-2022

Chang, R. Y.-W., Leck, C., Graus, M., Müller, M., Paatero, J., Burkhart, J. F., et al. (2011). Aerosol composition and sources in the central Arctic Ocean during ASCOS. *Atmospheric Chemistry and Physics*, *11*(20), 10619–10636. https://doi.org/10.5194/acp-11-10619-2011

Chang, R. Y.-W., Sjostedt, S. J., Pierce, J. R., Papakyriakou, T. N., Scarratt, M. G., Michaud, S., et al. (2011). Relating atmospheric and oceanic DMS levels to particle nucleation events in the Canadian Arctic. *Journal of Geophysical Research*, *116*(21), 1–10. https://doi.org/10.1029/2011JD015926

Chen, H., Ge, X., & Ye, Z. (2018). Aqueous-phase secondary organic aerosol formation via reactions with organic Triplet Excited States—A short review. *Current Pollution Reports*, *4*(1), 8–12. https://doi.org/10.1007/s40726-018-0079-7

Chen, L., Zhang, F., Zhang, D., Wang, X., Song, W., Liu, J., et al. (2022). Measurement report: Hygroscopic growth of ambient fine particles measured at five sites in China. *Atmospheric Chemistry and Physics*, *22*(10), 6773–6786. https://doi.org/10.5194/acp-22-6773-2022

Dionne, J., von Salzen, K., Cole, J., Mahmood, R., Leaitch, W. R., Lesins, G., et al. (2020). Modelling the relationship between liquid water content and cloud droplet number concentration observed in low clouds in the summer Arctic and its radiative effects. *Atmospheric Chemistry and Physics*, *20*(1), 29–43. https://doi.org/10.5194/acp-20-29-2020

Duplessis, P., Chang, R. Y.-W., Wheeler, M., Leaitch, W. R., & Svenningsson, B. (2023). Cloud condensation nuclei (CCN) concentration during the Arctic Ocean 2018 expedition. Bolin Centre Database, [Dataset]. https://doi.org/10.17043/oden-ao-2018-ccnc-1

Ervens, B., Turpin, B. J., & Weber, R. J. (2011). Secondary organic aerosol formation in cloud droplets and aqueous particles (aqSOA): A review of laboratory, field and model studies. *Atmospheric Chemistry and Physics*, *11*(21), 11069–11102. https://doi.org/10.5194/acp-11-11069-2011

Frey, M. M., Norris, S. J., Brooks, I. M., Anderson, P. S., Nishimura, K., Yang, X., et al. (2020). First direct observation of sea salt aerosol production from blowing snow above sea ice. *Atmospheric Chemistry and Physics*, *20*(4), 2549–2578. https://doi.org/10.5194/acp-20-2549-2020

Hamacher-Barth, E., Leck, C., & Jansson, K. (2016). Size-resolved morphological properties of the high Arctic summer aerosol during ASCOS-2008. *Atmospheric Chemistry and Physics*, *16*(10), 6577–6593. https://doi.org/10.5194/acp-16-6577-2016

Heintzenberg, J., Leck, C., Birmili, W., Wehner, B., Tjernström, M., & Wiedensohler, A. (2006). Aerosol number-size distributions during clear and fog periods in the summer high Arctic: 1991, 1996 and 2001. *Tellus Series B Chemical and Physical Meteorology*, *58*(1), 41–50. https://doi.org/10.1111/j.1600-0889.2005.00171.x

Held, A., Brooks, I. M., Leck, C., & Tjernström, M. (2011). On the potential contribution of open lead particle emissions to the central Arctic aerosol concentration. *Atmospheric Chemistry and Physics*, *11*(7), 3093–3105. https://doi.org/10.5194/acp-11-3093-2011

Intrieri, J. M., Shupe, M. D., Uttal, T., & McCarty, B. J. (2002). An annual cycle of Arctic cloud characteristics observed by radar and lidar at SHEBA. *Journal of Geophysical Research*, *107*(10). https://doi.org/10.1029/2000jc000423

IPCC. (2022): H.-O. Pörtner, D. C. Roberts, M. Tignor, E. S. Poloczanska, K. Mintenbeck, et al. (eds.). *Climate change 2022: Impacts, Adaptation, and Vulnerability. Contribution of working group II to the Sixth Assessment Report of the Intergovernmental panel on climate change*. Cambridge University Press, 3056 pp., https://doi.org/10.1017/9781009325844

Karl, M., Leck, C., Mashayekhy Rad, F., Bäcklund, A., Lopez-Aparicio, S., & Heintzenberg, J. (2019). New insights in sources of the sub-micrometre aerosol at Mt. Zeppelin observatory (Spitsbergen) in the year 2015. *Tellus Series B Chemical and Physical Meteorology*, *71*(1), 1–29. https://doi.org/10.1080/16000889.2019.1613143

Karlsson, L., Baccarini, A., Duplessis, P., Baumgardner, D., Brooks, I. M., Chang, R. Y.-W., et al. (2022). Physical and chemical properties of cloud droplet residuals and aerosol particles during the Arctic Ocean 2018 expedition. *Journal of Geophysical Research: Atmospheres*, *127*(11), 1–20. https://doi.org/10.1029/2021JD036383

Karlsson, L., Krejci, R., Koike, M., Ebell, K., & Zieger, P. (2021). A long-term study of cloud residuals from low-level Arctic clouds. *Atmospheric Chemistry and Physics*, *21*(11), 8933–8959. https://doi.org/10.5194/acp-21-8933-2021

Karlsson, L., Zieger, P., Salter, M., Dada, L., Schmale, J., Dällenbach, K., & Baccarini, A. (2022b). Cloud droplet residual and aerosol measurements from the Arctic Ocean 2018 expedition. Bolin Centre Database, [Dataset]. https://doi.org/10.17043/oden-ao-2018-aerosol-cvi-1

Köhler, H. (1936). The nucleus in and the growth of hygroscopic droplets. *Transactions of the Faraday Society*, *32*(1152), 1152–1161. https://doi.org/10.1039/TF9363201152

Koike, M., Ukita, J., Ström, J., Tunved, P., Shiobara, M., Vitale, V., et al. (2019). Year-round in Situ measurements of arctic low-level clouds: Microphysical properties and their relationships with aerosols. *Journal of Geophysical Research: Atmospheres*, *124*(3), 1798–1822. https://doi.org/10.1029/2018JD029802

Korhonen, H., Carslaw, K. S., Spracklen, D. V., Riley, D. A., & Ström, J. (2008). A global model study of processes controlling aerosol size distributions in the Arctic spring and summer. *Journal of Geophysical Research*, *113*(8), 1–20. https://doi.org/10.1029/2007JD009114

Lawler, M. J., Saltzman, E. S., Karlsson, L., Zieger, P., Salter, M., Baccarini, A., et al. (2021). New insights into the composition and origins of ultrafine aerosol in the summertime high arctic. *Geophysical Research Letters*, *48*(21), 1–11. https://doi.org/10.1029/2021GL094395

Leaitch, W. R., Korolev, A., Aliabadi, A. A., Burkart, J., Willis, M. D., Abbatt, J. P. D., et al. (2016). Effects of 20-100nm particles on liquid clouds in the clean summertime Arctic. *Atmospheric Chemistry and Physics*, *16*(17), 11107–11124. https://doi.org/10.5194/acp-16-11107-2016

Leck, C., & Bigg, E. K. (1999). Aerosol production over remote marine areas - a new route. *Geophysical Research Letters*, *26*(23), 3577–3580. https://doi.org/10.1029/1999gl010807

Leck, C., & Bigg, E. K. (2005). Biogenic particles in the surface microlayer and overlaying atmosphere in the central Arctic Ocean during summer. *Tellus B: Chemical and Physical Meteorology*, *57*(4), 305. https://doi.org/10.3402/tellusb.v57i4.16546

Leck, C., Matrai, P., Achtert, P., Adams, M., Baccarini, A., Brooks, B., et al. (2021). Data from expedition Arctic ocean, 2018. Bolin Centre Database Dataset. https://doi.org/10.17043/oden-ao-2018-expedition-1

Leck, C., Matrai, P., Perttu, A.-M., & Gårdfeldt, K. (2019). *Expedition report: SWEDARTIC Arctic Ocean 2018*. Swedish Polar Research Secretariat.

Leck, C., Norman, M., Bigg, E. K., & Hillamo, R. (2002). Chemical composition and sources of the high Arctic aerosol relevant for cloud formation. *Journal of Geophysical Research*, *107*(12). https://doi.org/10.1029/2001jd001463

Leck, C., & Svensson, E. (2015). Importance of aerosol composition and mixing state for cloud droplet activation over the Arctic pack ice in summer. *Atmospheric Chemistry and Physics*, *15*(5), 2545–2568. https://doi.org/10.5194/acp-15-2545-2015

Lohmann, U., & Leck, C. (2005). Importance of submicron surface-active organic aerosols for pristine Arctic clouds. *Tellus B: Chemical and Physical Meteorology*, *57*(3), 261. https://doi.org/10.3402/tellusb.v57i3.16534

Martin, M., Chang, R. Y.-W., Sierau, B., Sjogren, S., Swietlicki, E., Abbatt, J. P. D., et al. (2011). Cloud condensation nuclei closure study on summer arctic aerosol. *Atmospheric Chemistry and Physics*, *11*(22), 11335–11350. https://doi.org/10.5194/acp-11-11335-2011

Mauritsen, T., Sedlar, J., TjernstrÃm, M., Leck, C., Martin, M., Shupe, M., et al. (2011). An Arctic CCN-limited cloud-aerosol regime. *Atmospheric Chemistry and Physics*, *11*(1), 165–173. https://doi.org/10.5194/acp-11-165-2011

Orellana, M. V., Hansell, D. A., Matrai, P. A., & Leck, C. (2021). Marine polymer-gels' relevance in the atmosphere as aerosols and ccn. *Gels*, *7*(4), 1–17. https://doi.org/10.3390/gels7040185

Orellana, M. V., Matrai, P. A., Janer, M., & Rauschenberg, C. D. (2011). Dimethylsulfoniopropionate storage in phaeocystis (prymnesiophyceae) secretory vesicles. *Journal of Phycology*, *47*(1), 112–117. https://doi.org/10.1111/j.1529-8817.2010.00936.x

Ovadnevaite, J., Zuend, A., Laaksonen, A., Sanchez, K. J., Roberts, G., Ceburnis, D., et al. (2017). Surface tension prevails over solute effect in organic-influenced cloud droplet activation. *Nature*, *546*(7660), 637–641. https://doi.org/10.1038/nature22806

Petters, M. D., & Kreidenweis, S. M. (2007). A single parameter representation of hygroscopic growth and cloud condensation nucleus activity. *Atmospheric Chemistry and Physics*, *7*(8), 1961–1971. https://doi.org/10.5194/acp-7-1961-2007

Prytherch, J., & Tjernström, M. (2020). Navigation, meteorological and surface seawater data from the SWERUS-C3 Arctic Ocean expedition in 2014. Bolin Centre Database, Dataset version 2 https://doi.org/10.17043/oden-swerus-2014

Rantanen, M., Karpechko, A. Y., Lipponen, A., Nordling, K., Hyvärinen, O., Ruosteenoja, K., et al. (2022). The Arctic has warmed nearly four times faster than the globe since 1979. *Communications Earth and Environment*, *3*(1), 1–10. https://doi.org/10.1038/s43247-022-00498-3

Rissler, J., Preger, C., Eriksson, A. C., Lin, J. J., Prisle, N. L., & Svenningsson, B. (2023). Missed evaporation from atmospherically relevant inorganic mixtures confounds experimental aerosol studies. *Environmental Science and Technology*, *57*(7), 2706–2714. https://doi.org/10.1021/acs.est.2c06545

Rose, D., Gunthe, S. S., Mikhailov, E., Frank, G. P., Dusek, U., Andreae, M. O., & Pöschl, U. (2008). Calibration and measurement uncertainties of a continuous-flow cloud condensation nuclei counter (DMT-CCNC): CCN activation of ammonium sulfate and sodium chloride aerosol particles in theory and experiment. *Atmospheric Chemistry and Physics*, *8*(5), 1153–1179. https://doi.org/10.5194/acp-8-1153-2008

Schmale, J., Henning, S., Decesari, S., Henzing, B., Keskinen, H., Sellegri, K., et al. (2018). Long-term cloud condensation nuclei number concentration, particle number size distribution and chemical composition measurements at regionally representative observatories. *Atmospheric Chemistry and Physics*, *18*(4), 2853–2881. https://doi.org/10.5194/acp-18-2853-2018

Schmale, J., Sharma, S., Decesari, S., Pernov, J., Massling, A., Hansson, H. C., et al. (2022). Pan-Arctic seasonal cycles and long-term trends of aerosol properties from 10 observatories. *Atmospheric Chemistry and Physics*, *22*(5), 3067–3096. https://doi.org/10.5194/acp-22-3067-2022

Schmale, J., Zieger, P., & Ekman, A. M. L. (2021). Aerosols in current and future Arctic climate. *Nature Climate Change*, *11*(2), 95–105. https://doi.org/10.1038/s41558-020-00969-5

Screen, J., & Simmonds, I. (2010). The central role of diminishing sea ice in recent Arctic temperature amplification. *Nature*, *464*(7293), 1334–1337. https://doi.org/10.1038/nature09051

Sedlar, J., Tjernström, M., Mauritsen, T., Shupe, M. D., Brooks, I. M., Persson, P. O. G., et al. (2011). A transitioning Arctic surface energy budget: The impacts of solar zenith angle, surface albedo and cloud radiative forcing. *Climate Dynamics*, *37*(7–8), 1643–1660. https://doi.org/10.1007/s00382-010-0937-5

Shupe, M. D., & Intrieri, J. M. (2004). Cloud radiative forcing of the Arctic surface: The influence of cloud properties, surface albedo, and solar zenith angle. *Journal of Climate*, *17*(3), 616–628. https://doi.org/10.1175/1520-0442(2004)017<0616:CRFOTA>2.0.CO;2

Siegel, K., Karlsson, L., Zieger, P., Baccarini, A., Schmale, J., Lawler, M., et al. (2021). Insights into the molecular composition of semivolatile aerosols in the summertime central Arctic Ocean using FIGAERO-CIMS. *Environmental Sciences: Atmosphere*, *1*(4), 161–175. https://doi.org/10.1039/d0ea00023j

Siegel, K., Neuberger, A., Karlsson, L., Zieger, P., Mattsson, F., Duplessis, P., et al. (2022). Using novel molecular-level chemical composition observations of high arctic organic aerosol for predictions of cloud condensation nuclei. *Environmental Science and Technology*, *56*(19), 13888–13899. https://doi.org/10.1021/acs.est.2c02162

Spreen, G., Kaleschke, L., & Heygster, G. (2008). Sea ice remote sensing using AMSR-E 89-GHz channels. *Journal of Geophysical Research*, *113*(C2). https://doi.org/10.1029/2005jc003384

Stohl, A. (2006). Characteristics of atmospheric transport into the Arctic troposphere. *Journal of Geophysical Research*, *111*(11), 1–17. https://doi.org/10.1029/2005JD006888

Stohl, A., Aamaas, B., Amann, M., Baker, L. H., Bellouin, N., Berntsen, T. K., et al. (2016). Evaluating the climate and air quality impacts of short-lived pollutants. *Atmospheric Chemistry and Physics*, *15*(18), 10529–10566. https://doi.org/10.5194/acp-15-10529-2015

Svenningsson, B., Rissler, J., Swietlicki, E., Mircea, M., Bilde, M., Facchini, M. C., et al. (2006). Hygroscopic growth and critical supersaturations for mixed aerosol particles of inorganic and organic compounds of atmospheric relevance. *Atmospheric Chemistry and Physics*, *6*(7), 1937–1952. https://doi.org/10.5194/acp-6-1937-2006

Swietlicki, E., Zhou, J., Covert, D. S., Hämeri, K., Busch, B., Väkeva, M., et al. (2000). Hygroscopic properties of aerosol particles in the northeastern Atlantic during ACE-2. *Tellus Series B Chemical and Physical Meteorology*, *52*(2), 201–227. https://doi.org/10.3402/tellusb.v52i2.16093

Tjernström, M., Sedlar, J., & Shupe, M. D. (2008). How well do regional climate models reproduce radiation and clouds in the arctic? An evaluation of ARCMIP simulations. *Journal of Applied Meteorology and Climatology*, *47*(9), 2405–2422. https://doi.org/10.1175/2008JAMC1845.1

Von Der Weiden, S. L., Drewnick, F., & Borrmann, S. (2009). Particle Loss Calculator - a new software tool for the assessment of the performance of aerosol inlet systems. *Atmospheric Measurement Techniques*, *2*(2), 479–494. https://doi.org/10.5194/amt-2-479-2009

Vüllers, J., Achtert, P., Brooks, I. M., Tjernström, M., Prytherch, J., Burzik, A., & Neely, R. (2021). Meteorological and cloud conditions during the Arctic Ocean 2018 expedition. *Atmospheric Chemistry and Physics*, *21*(1), 289–314. https://doi.org/10.5194/acp-21-289-2021

Weingartner, E., Burtscher, H., & Baltensperger, U. (1997). Hygroscopic properties of carbon and diesel soot particles. *Atmospheric Environment*, *31*(15), 2311–2327. https://doi.org/10.1016/S1352-2310(97)00023-X

Wiedensohler, A. (1988). An approximation of the bipolar charge distribution for particles in the submicron size range. *Journal of Aerosol Science*, *19*(3), 387–389. https://doi.org/10.1016/0021-8502(88)90278-9

Wiedensohler, A., Birmili, W., Putaud, J.-P., & Ogren, J. (2013). Recommendations for aerosol sampling. *Aerosol Science: Technology and Applications*, 45–59.

Xu, W., Ovadnevaite, J., Fossum, K. N., Lin, C., Huang, R. J., Ceburnis, D., & O'Dowd, C. (2022). Sea spray as an obscured source for marine cloud nuclei. *Nature Geoscience*, *15*(4), 282–286. https://doi.org/10.1038/s41561-022-00917-2

Yang, X., Pyle, J. A., & Cox, R. A. (2008). Sea salt aerosol production and bromine release: Role of snow on sea ice. *Geophysical Research Letters*, *35*(16), 1–5. https://doi.org/10.1029/2008GL034536

Zábori, J., Rastak, N., Yoon, Y. J., Riipinen, I., & Ström, J. (2015). Size-resolved cloud condensation nuclei concentration measurements in the Arctic: Two case studies from the summer of 2008. *Atmospheric Chemistry and Physics*, *15*(23), 13803–13817. https://doi.org/10.5194/acp-15-13803-2015

Zieger, P., Fierz-Schmidhauser, R., Gysel, M., Stŕm, J., Henne, S., Yttri, K. E., et al. (2010). Effects of relative humidity on aerosol light scattering in the Arctic. *Atmospheric Chemistry and Physics*, *10*(8), 3875–3890. https://doi.org/10.5194/acp-10-3875-2010

Zieger, P., Väisänen, O., Corbin, J. C., Partridge, D. G., Bastelberger, S., Mousavi-Fard, M., et al. (2017). Revising the hygroscopicity of inorganic sea salt particles. *Nature Communications*, *8*, 15883. https://doi.org/10.1038/ncomms15883